ELSEVIER

Ceramics International 33 (2007) 1047–1052

CERAMICS INTERNATIONAL

www.elsevier.com/locate/ceramint

Synthesis of nanosized Nd:YAG powders via gel combustion

Jiang Li [a,b], Yubai Pan [a,*], Fagui Qiu [a,b], Yusong Wu [a,b], Wenbin Liu [a], Jingkun Guo [a]

[a] *State Key Lab of High Performance Ceramics and Superfine Microstructure, Shanghai Institute of Ceramics, Chinese Academy of Sciences, Shanghai 200050, PR China*

[b] *Graduate School of the Chinese Academy of Sciences, Beijing 100039, PR China*

Received 13 October 2005; received in revised form 2 February 2006; accepted 6 March 2006

Available online 3 July 2006

Abstract

Nanosized Nd:YAG powders with different doping concentrations were synthesized at a significantly low temperature by a gel combustion method with citric acid as fuel and nitrate as oxidizer. It is found that the precursor is composed of hydroxycarbonate and dehydrates at below 500 °C to form carbonate. Mono-phase Nd:YAG crystallites can be formed without any intermediate phase at 850 °C. The value of crystallite size of the 850 °C calcined 1.0 at% Nd:YAG powder is 59 nm and the average particle size is 86 nm. The doping of neodymium into YAG garnets increases the lattice constant and the fluorescent intensity decreases drastically when the neodymium concentration is higher than 3 at% because of the fluorescent quenching effect.

Keywords: Properties; Nanostructured Nd:YAG; Gel combustion synthesis

1. Introduction

The composition $3Y_2O_3{\cdot}5Al_2O_3$ commonly called yttrium alumina garnet (YAG, $Y_3Al_5O_{12}$) possesses the cubic garnet structure and when doped with neodymium YAG is an important solid-state laser material [1]. Conventionally, Nd:YAG is single crystal obtained by the Czochralski (CZ) method. Since Nd:YAG crystal was discovered first by Geusic et al. [2], the material has improved its optical properties rapidly and the Nd:YAG lasers have been applied with remarkable success to various industrial fields [3–6]. However, tens of days are required to grow a large size single crystal using the CZ method and it is extremely difficult to dope >1 at% neodymium homogeneously as a luminescence element in a YAG crystal [7,8], because the effective segregation coefficient of neodymium element for the YAG crystal is ~0.2, as reported in previously papers [9]. Furthermore, for melt growing a YAG single crystal, expensive Ir crucible has usually to be used and it is very difficult to get large size of samples.

Compared with Nd:YAG single crystals, polycrystalline Nd:YAG transparent ceramics have the advantages of being inexpensive and easy to fabricate, having a high-doped concentration, mass production and large size [10]. Recently, polycrystalline Nd:YAG ceramic laser materials have received much attention because the optical quality has been improved greatly and highly efficient laser oscillations could be obtained that comparable in efficiency with Nd:YAG crystals [11–18]. Heavily doped Nd:YAG ceramics are necessary for obtaining a high-power output laser. Owing to such application potential of Nd:YAG ceramics, some wet-chemical methods for the synthesis of pure and homogeneous YAG or Nd:YAG powders are adopted because of good mixing of the starting materials and excellent chemical homogeneity of the final products. These methods include sol-gel [19–22], precipitation [23–25], hydrothermal treatment [26–28], spray pyrolysis [29,30], combustion [31,32] and polymerized complex method [33]. Most of these methods suffer from complexity and time consuming procedures and/or mismatch in the solution behavior of the constituents.

However, gel combustion methods for synthesizing fine powders are of significant interest, primary due to the overall simplicity of the technique. Also the method can guarantee a precise control of cationic stoichiometry and homogeneous

* Corresponding author. Tel.: +86 21 52412820; fax: +86 21 52413903.
E-mail address: ybpan@mail.sic.ac.cn (Y. Pan).

0272-8842/$32.00
doi:10.1016/j.ceramint.2006.03.002

mixture of metal ions at the atomic level. In our previous work [34,35], pure YAG powders were prepared by the gel combustion method. Here, we report the preparation of Nd:YAG powders with different doping concentrations from a mixed-metal citrate–nitrate precursor by a simple gel combustion method at a relatively low temperature. The thermal behavior of the precursor, the phase transformation of the calcined powders, the micrographs of the precursor and the calcined powders, the lattice constant and the photoluminescence spectra of the gained Nd:YAG powders with different doping concentrations are investigated in this paper.

2. Experimental

Neodymium oxide was dissolved in concentrated nitric acid by stirring the mixture at 100 °C for 10 min in a beaker. Aluminum nitrate nonahydrate ($Al(NO_3)_3{\cdot}9H_2O$) and yttrium nitrate hexahydrate ($Y(NO_3)_3{\cdot}6H_2O$) dissolved in deionized water were added and the resulting mixtures were stirred at 60 °C for 30 min. The molar ratio of Nd:Y was controlled to 0.6, 1, 3, 4, 6 and 8%. The molar ratio of (Nd + Y):Al was kept as 3:5. In the mixed-metal nitrate solution, citric acid was added and the citrate-to-nitrate molar ratio γ was 1 (where $\gamma = M_{citrate}/M_{nitrate}$, M = molar amount of the compound). The mixed Y–Al–Nd citrate–nitrate aqueous solution was continuously stirred at 50–60 °C to obtain yellowish solution of the desired component. The solution was concentrated by evaporation at a solution temperature of ~80 °C under constant stirring, producing a transparent gel. A portion of this gel was collected for characterization. The gel was rapidly heated to 200 °C and the combusted products were calcined at various temperatures from 500 to 1100 °C in air for 2 h with a heating rate of 5 °C min^{-1}.

TG–DSC analysis was recorded on a Netzsch STA 449C instrument. Measurements were taken under a continuous flow of air (20 ml min^{-1}). Samples were heated at 10 °C min^{-1} to 1200 °C and then cooled to room temperature. The mass spectra (MS) of the gaseous products evolved from the samples in TG–DSC were simultaneously monitored with a Balzers Thermostar™ quadrupole mass spectrometer.

Phase identification was performed by a Rigaku D/max2200PC X-ray diffractometer (XRD) using nickel filtered Cu Kα radiation (1.5406 Å) in the range of $2\theta = 10–80°$. The tube current and voltage were 40 mA and 40 kV, respectively. The scanning speed was 4° min^{-1} and the step size was 0.02.

FTIR spectra of the as-prepared precursor and the calcined powders were measured on a Nicolet NEXUS 7000C spectrophotometer in the 400–4000 cm^{-1} range using the KBr pellet (~1 wt% sample) method. Each analysis consisted of a minimum 32 scans and the resolution was ±2 cm^{-1}.

Micrographs were taken using a JEOL JSM-6700 FESEM. Powders were dispersed in ethanol using an ultrasonic horn. Drops of the dispersed materials were deposited on a copper stub and dried in nature. Samples were sputter coated with palladium using a JEOL JFC-1600 auto fine coater system.

Specific surface area analyses were conducted at 77 K using a Norcross ASAP 2010 Micromeritics, with N_2 as the absorbate gas. Samples were degassed at 150 °C until the air pressure was

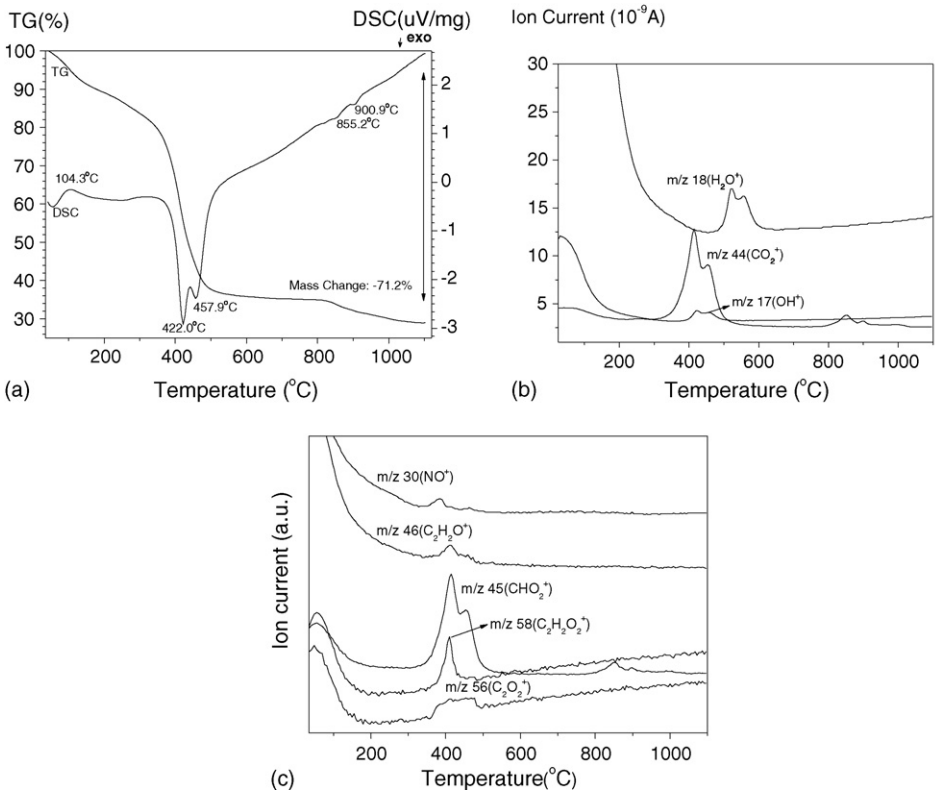

Fig. 1. (a) TG–DSC curve of the precursor; (b and c) mass spectra of characteristic ions from the precursor.

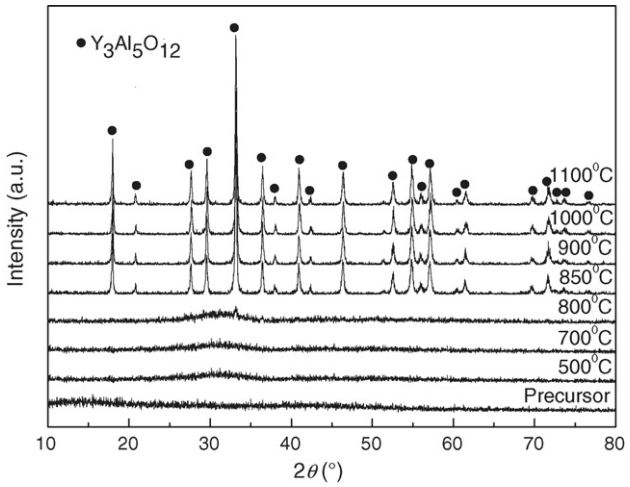

Fig. 2. The XRD patterns of the precursor and the powders calcined at various temperatures.

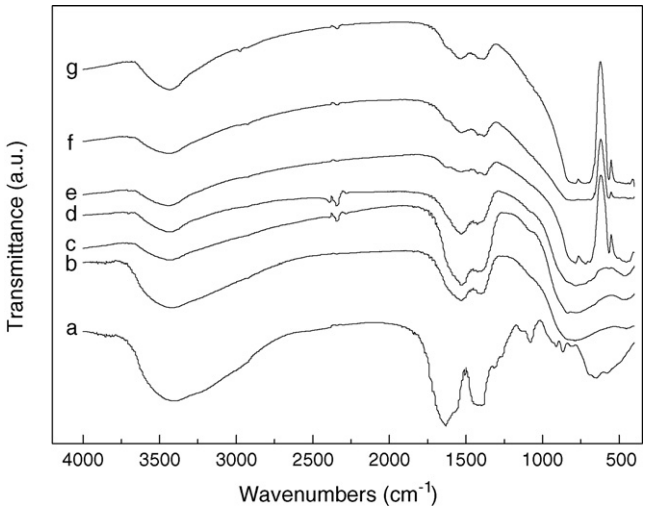

Fig. 3. FTIR spectra of (a) the precursor and the powders calcined at (b) 500 °C; (c) 700 °C; (d) 800 °C; (e) 850 °C; (f) 1000 °C; (g) 1100 °C.

below 5 μmHg. The specific surface areas were calculated using the BET multipoint method with eight data points.

Phase assemblages were determined by XRD using an XDC1000 Guinier–Hägg camera with Cu Kα radiation and Si as an internal standard. The measurement of X-ray film and refinement of lattice parameters were completed by a computer-linked line scanner (LS-18) system and the program PIRUM.

Photoluminescence (PL) spectra were recorded using a SPEX Fluorolog-3 modular spectrofluorometer employing a Hammatsu R5509-72 photomultiplier as the light detector, gratings with a groove density of 600 lines mm^{-1} and a 230 mW diode laser as the excitation source.

3. Results and discussion

The gel combustion synthesis involves a non-explosive exothermic reaction between metal nitrates and citric acid. The citrate–nitrate gel, after thermal dehydration, causes nitrate decomposition giving oxides of nitrogen (NO_x). The gaseous NO_x reacts with citrate generating heat and more gases.

3.1. Thermal analysis

Fig. 1 shows the TG–DSC curve and MS spectra of the precursor. A total mass loss of 71.2% indicates that the auto combustion reaction of the gel at 200 °C is incomplete. The infrared spectrum of precursor indicates the presence of a hydroxyl group and the carbonate group therein Fig. 3. It is considered that precursor is composed of hydroxycarbonate contaminated with unburnt carbon. A sharp weight loss appears at temperature range of 350–500 °C in TG curve and two distinct exothermic peaks are detected in the DSC curve, as shown in Fig. 1(a). The substantial mass loss results from the release of CO_2, H_2O and NO gases due to the decomposition of the precursor, as detected by the mass spectra (Fig. 1(b and c)). The NO signal in the course of decomposition may come from the residual nitrate during the combustion reaction. Some organic groups such as $OH^+(m/z = 17)$, $C_2H_2O^+(m/z = 42)$, $CHO_2^+(m/z = 45)$, $C_2O_2^+(m/z = 56)$ and $C_2H_2O_2^+(m/z = 58)$ are observed in the mass spectra at temperature range of 350–500 °C, which is probably related to the fragments of citrate or citric acid. Considering the infrared spectrum in Fig. 3, it can be supposed that hydroxycarbonate of the precursor dehydrates at below 500 °C to form carbonate. Close observation shows that two small exothermic peaks appear at 855.2 and 900.9 °C, respectively. It can be consider that the former results from the crystallization of amorphous Nd:YAG and the latter is attributed to the oxidation of free carbon impurity. This conclusion can be supported by the results of XRD patterns in Fig. 2 and mass spectra in Fig. 1(b). The mentioned mass loss of 71.2% is higher than a theoretically calculated value (∼41.8%) for the transformation of hydroxycarbonate dehydrates to 1.0 at% Nd:YAG, as is due to the existence of excess citric acid and carbon from incomplete combustion of citrate.

3.2. Phase analysis by XRD

XRD patterns of the precursor and the powders calcined at different temperatures are shown in Fig. 2. Since no obvious diffraction peaks are observed, it can be concluded that the precursor and the powders from the precursor calcined below 800 °C are amorphous in nature. At 800 °C, the strongest characteristic peak of Nd:YAG phase appears with rather weak intensity, indicating the crystallization of amorphous Nd:YAG. With increase of the calcination temperature up to 850 °C, high and sharp peaks observed indicate the improved crystallinity of Nd:YAG. Therefore, it can be considered that Nd:YAG crystallizes directly from the amorphous phase without any intermediate phase. Crystallite size of the 850 °C calcined powder is determined by X-ray line broadening and calculated using the Scherrer equation:

$$d_{\mathrm{Crys}} = \frac{0.89\lambda}{B\cos\theta}$$

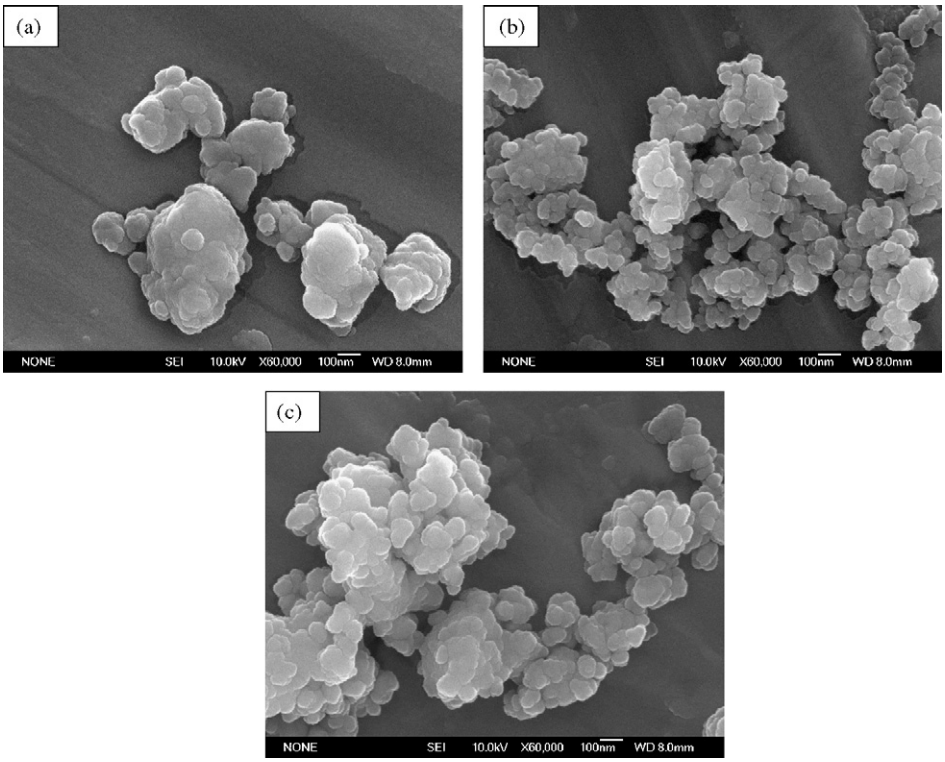

Fig. 4. FESEM micrographs of (a) the precursor and the powders calcined at (b) 850 °C; (c) 900 °C.

where

$$B = (B_o^2 - B_c^2)^{1/2}$$

where B_o is the full width at half maximum (in 2θ (°)), B_c the correction factor for instrument broadening, θ the peak maximum (in 2θ (°)), and λ is the Cu Kα weighted average wavelength. The value of crystallite size calculated from the (4 2 0) XRD peak is 59 nm. At the temperatures higher than 850 °C, higher intensities of Nd:YAG peaks are observed, indicating crystallite growth of the Nd:YAG grains.

3.3. Infrared spectra analyses

Fig. 3 shows the FTIR spectra of the precursor and the powders from the precursor calcined at various temperatures. The spectrum of the precursor clearly shows a broad absorption around 3450 cm^{-1}, which is a characteristic stretching vibration of hydroxyl groups (O–H). Peaks localized at 1636 and 1395 cm^{-1} are assigned to asymmetrical and symmetrical stretching vibration of carboxylate (O–C=O), respectively. For the powder calcined at 500 °C, the spectrum reveals that the carboxylate of the precursor transforms into the carbonate with the characteristic asymmetrical split stretching localized at 1535 and 1403 cm^{-1}. For the powder calcined at 850 °C, the characteristic absorption bands of YAG appear, as is in agreement with the result of XRD mentioned above. Absorption bands at 1535 and 1378 cm^{-1} may be caused by the absorption of H_2O and CO_2 in the synthesized powder. All samples show intensive O–H vibration band even they were annealed at higher temperatures. It is also caused by the absorption of H_2O in air. There are no significant changes in the FTIR spectra with further increase of calcination temperature.

3.4. FESEM and HRTEM analysis

Fig. 4 shows the FESEM micrographs of the precursor and the powders from the precursor calcined at different temperatures. The morphology of the as-synthesized precursor is depicted in Fig. 4(a). The nature of the agglomerates in the precursor indicates the existence of carboxylate. Upon calcinations, they crystallize and their shape becomes more discrete at 850 °C, as shown in Fig. 4(b). The specific surface area of the 850 °C calcined powder is 16.17 m^2/g. The particle average size is derived from the formula with d_{BET} being the average particle size, ρ the density of the material, and S_{ssa} its specific surface area.

$$d_{BET} = \frac{6}{\rho S_{ssa}}$$

Particle size obtained using the above formula is 86 nm. It can be concluded that the agglomeration scope in the corresponding powder is relatively lower according to the crystallite size calculated above.

It is shown in Fig. 4(c) that as calcination temperature goes up to 900 °C, the crystallite and the agglomerate size in the corresponding powder become bigger. There is a tendency the boundary of the individual crystallites becomes more discernible. Fig. 5 shows the HRTEM lattice image of the powder calcined at 850 °C. It can be seen that the Nd:YAG powder is well-crystallized, which supports both the XRD and FTIR observations in Figs. 2 and 3.

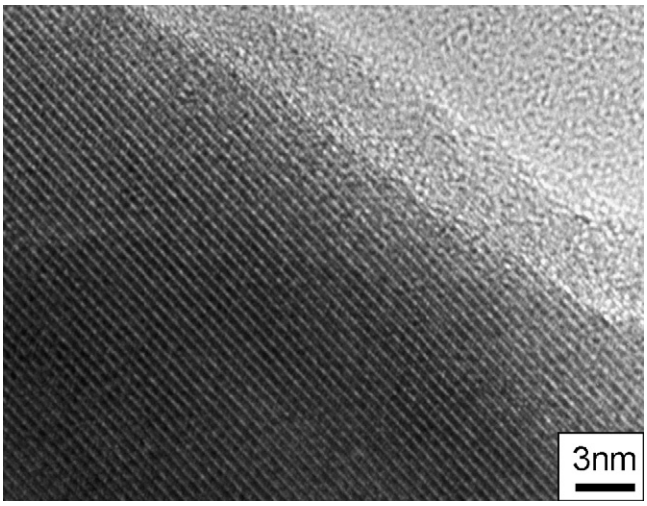

Fig. 5. HRTEM micrograph of the powder calcined at 850 °C.

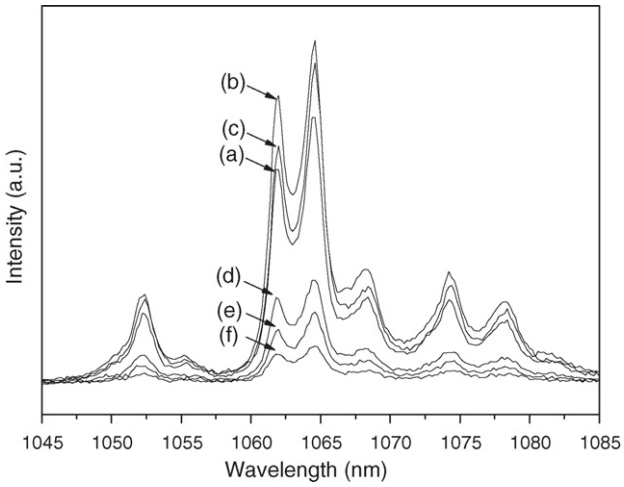

Fig. 7. Photoluminescence emission spectra of Nd:YAG powders with different doping concentrations (a) 0.6 at%; (b) 1.0 at%; (c) 3.0 at%; (d) 4.0 at%; (e) 6.0 at%; (f) 8.0 at% (under excitation of 808 nm radiation).

3.5. Lattice constant

The fully crystallized phase is identified as garnet structure for powders after being calcined at 850 °C. The cell constants calculated from the XRD patterns are 12.0598, 12.0612, 12.0619, and 12.0703 Å for 0, 0.6, 1.0, and 3.0 at% Nd:YAG, respectively. The values are greater than what theoretically they should be (a = 12.02 Å for YAG, JCPDS No. 82-0575). The reason may be caused by the powder consisting of nanoparticles, which results in the lattice expansion [22,36].

The relationship between the lattice parameters and the Nd concentration is shown in Fig. 6. It does not present the strictly linear relationship. Because the effective radius of Nd^{3+} (0.983) is bigger than that of Y^{3+} (0.900) [37], doping Nd into YAG garnets will increase the crystal lattice and lead to the structure deformation.

3.6. Photoluminescence spectra

The room-temperature photoluminescence emission spectra for $^4F_{3/2}$ to $^4I_{11/2}$ transition of Nd:YAG powders with different doping concentrations are illustrated in Fig. 7. It can be seen that the main fluorescence peaks are all near 1064.6 nm for 0.6, 1.0, 3.0, 4.0, 6.0 and 8.0 at% Nd:YAG powders, respectively. The fluorescent intensity improves when the doping concentration increases from 0.6 to 1.0 at%. There is a slight decrease in intensity when the neodymium concentration increases to 3.0 at%. However, fluorescent intensity decreases drastically with further increase of neodymium concentration because of the fluorescent quenching effect. No obvious wavelength redshift has been observed with increasing the neodymium concentration. The fluorescent line widths for 0.6, 1.0 and 3.0 at% Nd:YAG powders are almost identical. It means the fluorescent quenching effect is very weak for neodymium concentration lower than 3 at%, which is much higher than that of Nd:YAG single crystals. The fluorescent line width at 1064.6 nm is also a little broadened with the concentration increases greater than 3.0 at% due to the quenching effect.

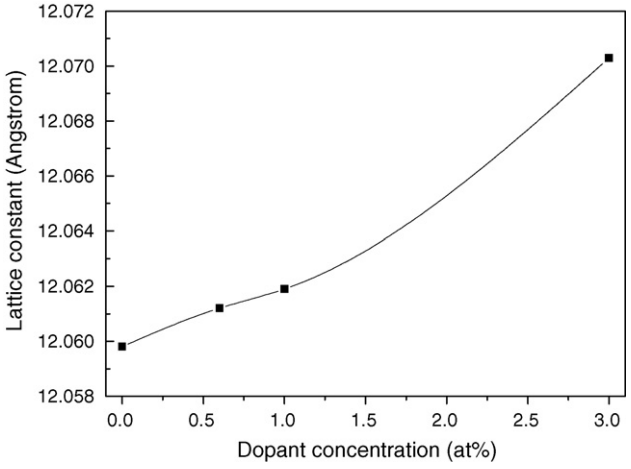

Fig. 6. Plot of the lattice constant with Nd doping concentrations in YAG.

4. Conclusions

Nanosized Nd:YAG powders with different doping concentrations were synthesized by a gel combustion method with citrate-to-nitrate ratio $\gamma = 1$. The precursor composed of hydroxycarbonate dehydrates below 500 °C to form carbonate. Mono-phase Nd:YAG powders can be obtained at 850 °C without forming any intermediate phase. The crystallite size of the 850 °C calcined 1.0 at% Nd:YAG powder is 59 nm and the average particle size is 86 nm. With increase of calcination temperature, the crystallite and the agglomerate size in the corresponding powder become bigger. The doping of neodymium into YAG garnets increases the lattice constant and leads to the structure deformation. The main fluorescence peaks are all near 1064.6 nm for Nd:YAG powders with different doping concentrations. The fluorescent quenching effect is very weak for neodymium concentration lower than 3 at%. The highly pure, relatively homogeneous and high doping concentration Nd:YAG powders are desirable to prepare transparent polycrystalline Nd:YAG ceramics as solid-state laser materials.

Acknowledgements

This work was supported by the Applied Basic Research Programs of Science and Technology Commission Foundation of Shanghai (Grant No. 05DZ22005) and the Key Project of Science and Technology of Shanghai (Grant No. 04DZ14002). We are grateful to Mr. Chundong Wu for the assistance in XRD and FTIR studies. The authors show great appreciation to Dr. Changming Xu and Dr. Lu Gao for helpful discussion.

References

[1] J.J. Zayhowski, Passively *Q*-switched Nd:YAG microchip lasers and applications, J. Alloy Compd. 303–304 (2000) 393–400.
[2] J.E. Geusic, H.M. Marcos, L.G. Van Uitert, Laser oscillation in Nd-doped yttrium aluminum, yttrium gallium and gadolinium garnets, Appl. Phys. Lett. 4 (10) (1964) 182–184.
[3] N. Daikuzono, Present and future of medical YAG laser, Rev. Laser Eng. 21 (8) (1993) 894–895.
[4] N. Goto, H. Ito, High-average-power 266 nm generation of Nd:YAG laser and its industrial application, Rev. Laser Eng. 21 (8) (1993) 885–893.
[5] K. Ueda, N. Uehare, Frequency stabilization of LD-pumped YAG laser for gravitational wave detection, Rev. Laser Eng. 21 (8) (1993) 859–872.
[6] M. Doshida, H. Saito, The obstale waring lidar system using LD pumped Nd:YAG laser, Rev. Laser Eng. 21 (8) (1993) 899–905.
[7] T. Sekino, Y. Sogabe, Progess in the YAG crystal growth technique for solid state lasers, Rev. Laser Eng. 21 (8) (1993) 827–831.
[8] H. Hayakawa, H. Umino, M. Mori, H. Fujii, Ovservation of striations in Nd:YAG with circularly polarized light, Jpn. J. Appl. Phys. 24 (8) (1985) L614–L616.
[9] R.R. Monchamp, The distribution coefficient of neodymium and lutetium in Czochralski brown $Y_3Al_5O_{12}$, J. Cryst. Growth 11 (1971) 310–312.
[10] J. Lu, K. Ueda, H. Yagi, T. Yanagitani, A. Kudryashov, A.A. Kaminskii, Potential of ceramic YAG lasers, Laser Phys. 11 (10) (2001) 1053–1057.
[11] A. Ikesue, I. Furusato, K. Kamata, Fabrication of polycrystallin, transparent YAG ceramics by a solid-state reaction method, J. Am. Ceram. Soc. 78 (1) (1995) 225–228.
[12] A. Ikesue, T. Kinoshita, K. Kamata, K. Yoshida, Fabrication and optical properties of high-performance polycrystalline Nd:YAG ceramics for solid-state lasers, J. Am. Ceram. Soc. 78 (4) (1995) 1033–1040.
[13] A. Ikesue, K. Yoshida, Influence of pore volume on laser performance of Nd:YAG ceramics, J. Mater. Sci. 34 (1999) 1189–1195.
[14] I. Shoji, S. Kurimura, Y. Sato, T. Taira, Optical properties and laser characteristics of high Nd^{3+}-doped $Y_3Al_5O_{12}$ ceramics, Appl. Phys. Lett. 77 (7) (2000) 939–941.
[15] J. Lu, M. Prahu, J. Song, C. Li, J. Xu, K. Ueda, A.A. Kaminskii, H. Yagi, T. Yanagitani, Optical properties and highly efficient laser oscillation of Nd:YAG ceramics, Appl. Phys. Lett. B 71 (2000) 469–473.
[16] J. Lu, M. Prahu, J. Xu, K. Ueda, H. Yagi, T. Yanagitani, A.A. Kaminskii, Highly efficient 2% Nd:Yttrium alumina garnet ceramic laser, Appl. Phys. Lett. 77 (23) (2000) 3707–3709.
[17] J. Lu, J. Song, M. Prabhu, J. Xu, K. Ueda, H. Yagi, T. Yanagitani, A. Kudryashov, High-power Nd:$Y_3Al_5O_{12}$ ceramic laser, Jpn. J. Appl. Phys. Lett. 39 (2000) L1048–L1050.
[18] J. Lu, M. Prahu, J. Xu, K. Ueda, H. Yagi, T. Yanagitani, A.A. Kaminskii, Highly efficient Nd:YAG $Y_3Al_5O_{12}$ ceramic laser, Jpn. J. Appl. Phys. Lett. 40 (2001) L552–L554.
[19] G. Gowda, Syntehsis of yttrium aluminates by the Sol–gel process, J. Mater. Sci. Lett. 5 (10) (1986) 1029–1032.
[20] R. Manalert, M.N. Rahaman, Sol–gel process and sintering of yttrium aluminum garnet (YAG) powders, J. Mater. Sci. 31 (1996) 3453–3458.
[21] H.M. Wang, M.C. Simmonds, J.M. Rodenburg, Manufacturing of YbAG coatings and crystallisation of the pure and Li_2O-doped Yb_2O_3–Al_2O_3 system by a modified sol–gel method, Mater. Chem. Phys. 77 (2003) 802–807.
[22] H.M. Wang, M.C. Simmonds, Y.Z. Huang, J.M. Rodenburg, Synthesis of nanosize powders and thin films of Yb-doped YAG by sol–gel methods, Chem. Mater. 15 (2003) 3474–3480.
[23] J.W.G.A. Vrolijk, J.W.M.M. Willens, R. Metselaar, Coprecipitation of yttrium and aluminum hydroxide for preparation of yttrium aluminum garnet, J. Eur. Ceram. Soc. 6 (1990) 47–53.
[24] D.J. Sordelet, M. Akinc, M.L. Panchula, Y. Han, M.H. Han, Synthesis of yttrium aluminum garnet precursor powders by homogeneous precipition, J. Eur. Ceram. Soc. 14 (1994) 123–130.
[25] N. Matsushita, N. Tsuchiya, K. Nakatsuka, T. Yanagitani, Precipitation and calcination process for yttrium aluminum garnet precursor powders synthesized by the urea method, J. Am. Ceram. Soc. 82 (8) (1999) 1977–1984.
[26] T. Takamori, L.D. David, Controlled nucleation for hydrothermal growth of yttrium aluminum garnet powders, J. Am. Ceram. Soc. 65 (9) (1986) 1282–1286.
[27] Y. Hakuta, T. Haganuma, K. Sue, T. Adschiri, K. Arai, Continuous production of phosphor YAG:Tb nanoparticles by hydrothermal synthesis in supercritical water, Mater. Res. Bull. 38 (2003) 1257–1265.
[28] M. Inoue, H. Otsu, H. Kominami, T. Inui, Synthesis of yttrium aluminum garnet by the glycothermal method, J. Am. Ceram. Soc. 74 (6) (1991) 1452–1454.
[29] M. Nyman, J. Caruso, M.J. Hampden-Smith, T.T. Kodas, Comparasion of solid-state and spray-pyrolysis of yttrium aluminate powders, J. Am. Ceram. Soc. 80 (5) (1997) 1231–1238.
[30] Y.C. Kang, I.W. Lenggoro, S.B. Park, K. Okuyama, YAG:Ce phosphor particles prepared by ultrasonic spray pyrolysis, Mater. Res. Bull. 35 (2000) 789–798.
[31] K.T. Pillar, R.V. Kamat, V.N. Vaigya, D.D. Sood, Synthesis of yttrium aluminum garnet by the glycerol route, Mater. Chem. Phys. 44 (1996) 255–260.
[32] S. Shi, J. Wang, Combustion synthesis of Eu^{3+} activated $Y_3Al_5O_{12}$ phosphor nanoparticles, J. Alloy Compd. 327 (2001) 82–86.
[33] B.H. King, J.W. Halloran, Polycrystalline yttrium aluminum garnet fibers from colloidal sols, J. Am. Ceram. Soc. 7 (8) (1995) 2141–2148.
[34] F.G. Qiu, X.P. Pu, J. Li, X.J. Liu, Y.B. Pan, J.K. Guo, Thermal behavior of the YAG precursor prepared by sol–gel combustion process, Ceram. Int. 31 (2005) 663–665.
[35] F.G. Qiu, X.P. Pu, R. Zhang, J.K. Guo, Low-temperature synthesis of mono-phase ultrafine yttrium aluminum garnet by sol–gel combustion process, Key Eng. Mater. 280–283 (2005) 717–720.
[36] R. Lamber, S. Wetjen, N.I. Jaeger, Size dependence of the lattice parameter of small palladium particles, Phys. Rev. B 51 (1995) 10968–10971.
[37] R.D. Shannon, Revised effective ionic radii and systematic studies of interatomic distances in halides and chalcogenides, Acta Crystallogr. A 32 (1976) 751–767.